

ENHANCED SPATIAL RESOLUTION USING ITERATIVE FOCAL DESMEARING IN COMPUTED TOMOGRAPHY

Axel LANGE, Manfred P. HENTSCHEL, Andreas KUPSCH

BAM FEDERAL INSTITUTE FOR MATERIALS RESEARCH AND TESTING,
12200 Berlin, Germany

Abstract

Computed tomography reconstructions of projected data usually assume an ideal point-like focal spot. However, in practice, the actual finite focus size leads to blurred projections, unavoidably. The elements (voxels) of the reconstruction array are smeared differently as a function of their individual position relative to source and detector. Neglecting the focal smearing generates considerably blurred reconstructions. Previous attempts were based on directly deconvolving blurred projections from a constant kernel, which yields better results but still exhibits artefacts. Iterative algorithms can be adopted to take into account focal smearing as a function of position. However, this requires detailed prior knowledge of quantitative smear functions. The DIRECTT (Direct Iterative Reconstruction of Computed Tomography Trajectories) algorithm is a promising candidate to meet these requirements. It has been demonstrated elsewhere that DIRECTT copes with limited data sets such as limited view and region-of-interest data by tracing single sinusoidal-like trajectories in Radon space, which are selected from the set of all possible trajectories by appropriate criteria. Currently, position-dependent smearing is used in the projection part of iterations. At the example of model reconstructions we demonstrate the gain of spatial resolution by iterative variable desmearing according to the DIRECTT algorithm in comparison to the standard filtered back-projection.

1 Introduction

A general bottle neck of radiology is unavoidable blurring of projection images caused by the finite focus size of the radiation source. This drawback occurs independent of the type of radiation. It refers to X-rays as well as gammas, electrons, neutrons, and Terahertz waves. However, in practical materials testing, radiology using X-ray sources is the most prevalent technique. In order to get a measure of the momentousness of the focal spot size problem one may consider the optimization efforts made by tube manufacturers and provider of CT complete systems: maximal integral output power should be achieved from smallest possible focal spot sizes.

Needless to say that tomograms, which consist of a series of radiographs, suffer from the same problem since achievable quality of reconstructions is essentially determined by the (spatial) resolution of the input data, i.e. the single projections.

Experimental background of the following study are tomographic measurements using neutrons, where the mentioned problem emerges in a tremendous way. Thermal neutrons generated by a research reactor are employed in order to localize water condensates in 3D space in PEM fuel cells, which consist of metallic components and housing (PEM: Polymer Electrolyte Membrane, or Proton Exchange Membrane, for the operating principle of PEM fuel cells refer to [1-3]).

Unlike the X-ray attenuation coefficient, the attenuation of thermal neutrons is no monotone function of the atomic number. Certain chemical elements such as hydrogen, gadolinium, or cadmium exhibit a strong absorption. Concerning neutrons the term 'focus'

is replaced by ‘aperture’, ‘neutron flux’ instead of ‘intensity’. However, the general geometric reasons for blurred projections and the additivity of attenuation coefficients remain unchanged.

In order to obtain a sufficient neutron flux (to ensure sufficient statistics) the aperture must not exceed a minimal size. In practical applications apertures are in the order of some centimetres, i.e. the (unwanted) effect of focal blurring has a larger impact compared to conventional X-ray sources. Since miniaturization of the aperture is to be discarded for the reasons mentioned above, the only way out are numerical solutions (or approximations at least).

2 Position dependent smearing

The basic geometric assumption of numerically modeling blurred projections is analogously to the calculation of variable magnification (of single pixels or voxels in a discretized reconstruction space) in fan or cone beam projections given by the intercept theorems.

Here, however, the respective pixel is the apex of rays instead of the (ideally point-like) source (see Fig. 1): each single pixel is considered as a pinhole camera, which projects the source (of finite size). Quantitatively, the smear function’s width V_s can be denoted as

$$V_s(AQA) = \frac{AQD - AQA}{AQA} = \frac{AQD}{AQA} - 1. \quad (1)$$

The assignment of relevant distances AQA (distance source-axis) and AQD (distance source-detector) can be seen from Fig. 1. As a straight result of equ. (1) the smearing width approaches zero in the limit $AQA \rightarrow AQD$, i.e. a contact radiograph is inherently sharp.

While variation of the magnification changes the (well defined) detector position of the respective projected mass element (voxel) the smearing (essentially its width) describes the voxel’s weighted distribution on an interval of detector positions.

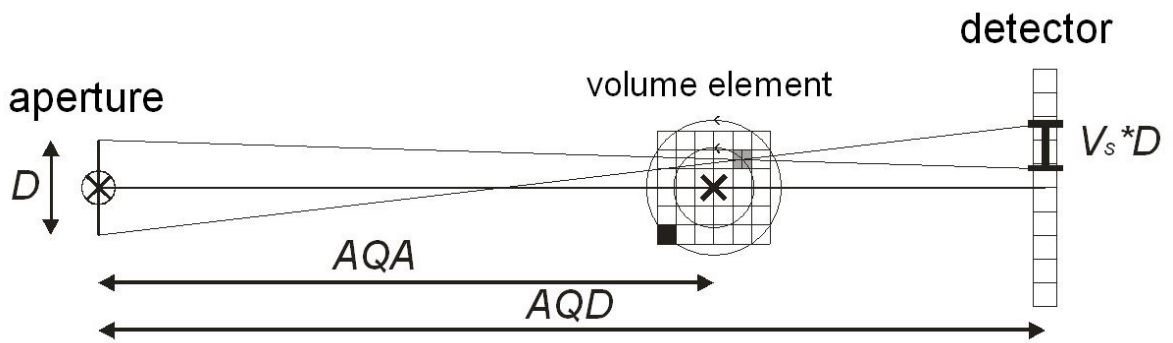


Fig. 1: Geometric fundamentals of focal blurring of single pixels caused by finite source size. Quantitative smearing is expressed relative to the aperture D .

Both, smearing and magnification are independent of the lateral position, i.e. the voxel’s position within an arbitrary plane perpendicular to the central beam. In the following we will use the term ‘position’ which indicates a voxel’s position relative to source and detector, i.e. its projection on the central beam.

The smear width of a pixel P_0 with a distance R_0 from the rotation axis is denoted as a function of projection angle φ :

$$V_s(\varphi) = \frac{AQD - (AQA + R_0 \cos \varphi)}{AQA + R_0 \cos \varphi}. \quad (2)$$

$V_s(\varphi)$ passes through a minimum at $\varphi = 0$ (near the detector), and a maximal value at $\varphi = \pi$ (maximum distance from the detector). This is visualized in the polar plot in Fig. 2. The parameters assumed are those of real neutron tomographic measurements of a complete fuel cell: $AQD = 6000$ mm, $AQA = 5800$ mm, and $R_0 = 50$ mm. In order to achieve a minimal smearing the fuel cell is placed in close vicinity of the detector. Its lateral size l of about 100 mm leads to the maximal radius R_0 on the one hand, on the other hand a full rotation of the fuel cell (incl. external gas supply) must be performed without touching the detector: $AQD - AQA > l/2$. By applying these parameters one calculates a variation of smear width of 70% for a full rotation while the magnification changes for just 2%.

As a first approximation the position dependent smear function can be assumed as a Gaussian kernel (Fig. 2 left). According to equ. (1) its width increases with the distance from the detector $t (=AQD - AQA)$. However, concerning measured data the smear width as function of position must be determined experimentally. A sharp edge (ideal Heaviside step function) made of a strong absorber, which is prepared as thin slab, is suited for purely investigating this effect.

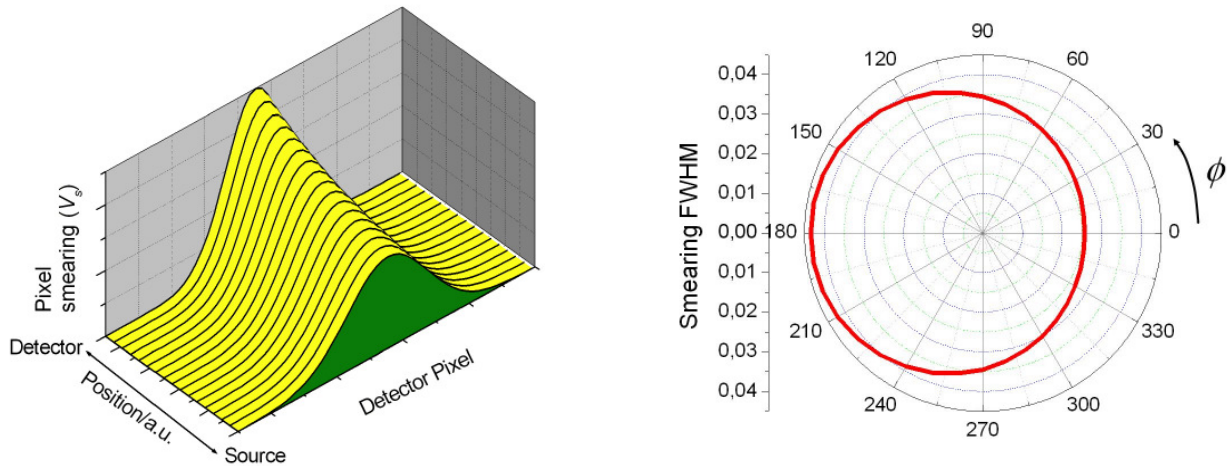


Fig. 2: Variation of a Gaussian kernel as a function of position (left, the integral is a conserved quantity) and polar plot of the variable smear width for a full rotation of a selected pixel (right, cf. equ. (2)).

With the prior knowledge of position dependent smearing the blurred projection of a known object can be computed, which is essential for simulating the proper mode of operation of the smear procedure. Fig. 3 (right) illustrates this mode of operation: elements close to the detector (t small) are sparsely smeared, elements far off the detector stronger. This becomes obvious with a view to the vertical ($\parallel t$) lines and the parallel edges and edge segments of the triangles and circles. In contrast a constant smearing (Fig. 3 centre) blurs elements at all positions with same width (as an example the mean value of smearing is applied).

Since the measurement (single projection) represents an integral value, i.e. the sum over all variably smeared positions t (Fig. 3 bottom), the resulting blurring cannot be removed by simple deconvolution (implicitly: the generation of an unsmeared sinogram) since no information about the respective position is available.

The terms 'smearing' and 'convolution' (and their respective inverse operations) are differentiated by the distinct application of convolution kernels. 'Smearing' means: at each position the sharp projection is subject to a local convolution (i.e. with locally constant kernel). Applying a globally constant kernel (i.e. the kernel is not a function of position) is

called a ‘convolution’; the measured projections can be deconvolved directly. The analogue inverse operation of ‘smearing’ of a projection (i.e. ‘desmearing’) cannot be computed analytically.

However, it will be demonstrated in the following, that one can succeed in *iterative* ‘desmearing’ a series of projections (e.g. a tomogram), by *proper projecting* (i.e. applying the proper smearing) the irradiated object, whose shape and inner structure (mass distribution) is better known in each step of iteration.

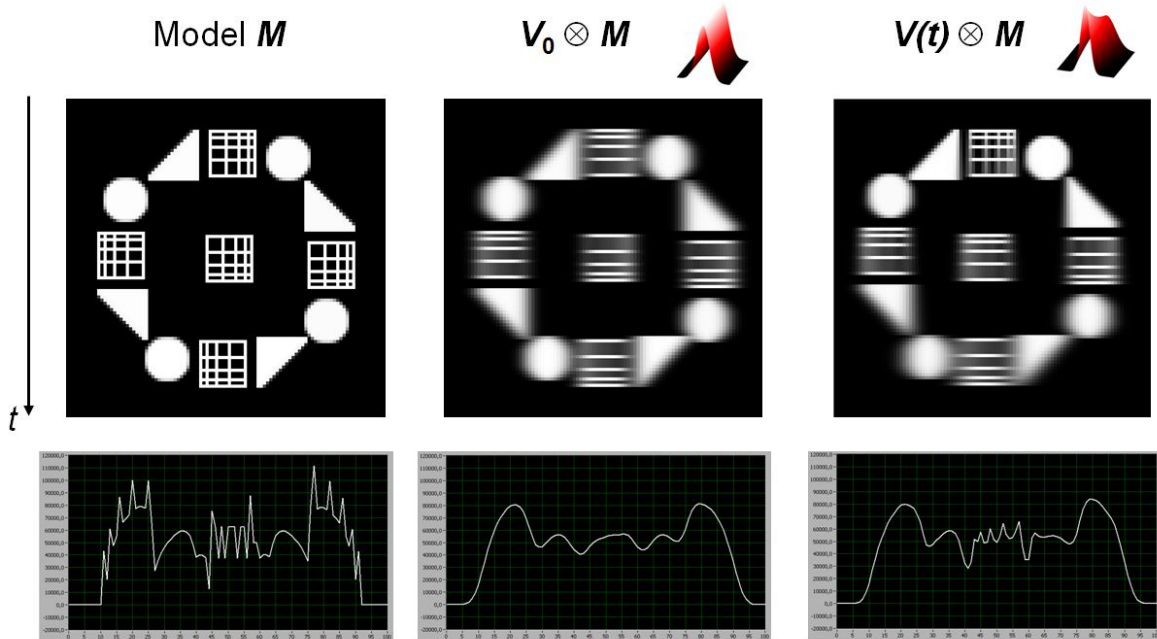


Fig. 3: Effects of different smear functions on single projections of model **M**: ideal projection (left), constant (centre) and variable position-dependent smearing (right, the parameter t indicates the distance from the detector). Bottom: integration in t direction provides the respective projection profiles (sinogram line 0 in Fig. 5).

3 Iterative reconstruction: DIRECTT

The described approach of computing the position dependent smearing is meant to improve the reconstruction results of considerably smeared CT measurements. It is optionally implemented to the DIRECTT algorithm (Direct Iterative Reconstruction of Computed Tomography Trajectories) [4], which has been reported elsewhere [5,6]. The algorithm is applicable for parallel, fan and cone beam geometry CT and been shown to yield better reconstruction results than the conventional Filtered Back-Projection (FBP) [7], in particular with respect to limited data sets such as *Limited View* or *Region of Interest* data. At least two of DIRECTT’s drawing cards meet the requirements of implementing the position dependent focal smearing: (a) the precise projection and (b) the algorithm’s iterative conception.

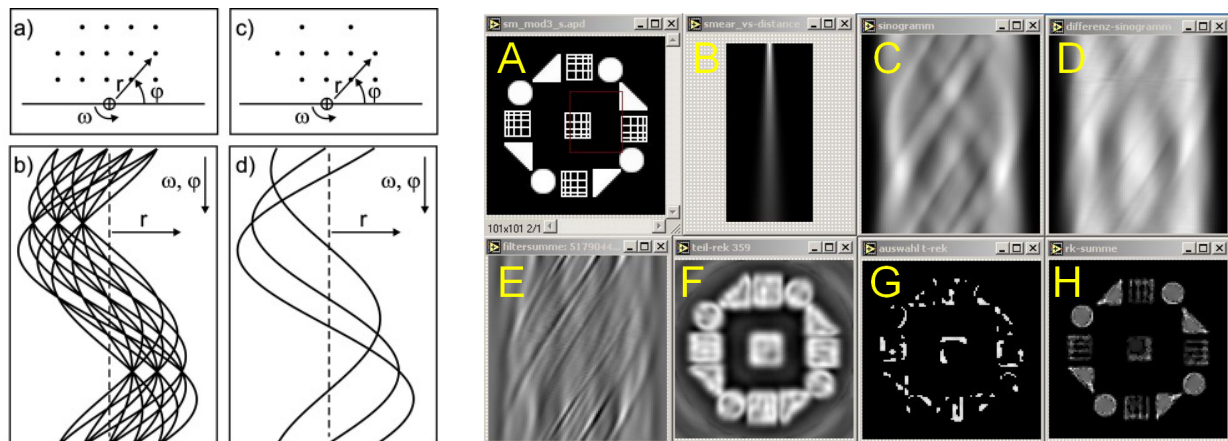


Fig. 4: DIRECTT principle (left) and stages of the iteration procedure (right).

Fig. 4 (left) schematically illustrates DIRECTT's course of iterations. Fig. 4a (top left) displays a model at the example of a phantom consisting of 14 single elements. Fig. 4b (bottom left) depicts the respective sinogram (Radon transform [8]), which is either the projection of an (exemplary) mass distribution (Fig. 4a), a partial reconstruction or the experimental data set.

Considering the fact that each element of the reconstruction array corresponds to exactly one sinusoidal trajectory of the sinogram the DIRECTT algorithm evaluates the weight and contrast of all possible trajectories (Fig. 4b) and selects those of predominant weight or contrast (averaged over all angles). The respective reconstruction elements are added to the reconstruction array (Fig. 4c, 11 out of the 14 original elements in the example). The projection (Radon transform) of these elements (i.e. a computed sinogram) is then subtracted from the original data set. The obtained residual sinogram (Fig. 4d, containing trajectories of 3 remaining elements in the example) is subject to the same procedure in the subsequent iteration steps until a pre-selected criterion of convergence is reached. This procedure can be described as an iterative Radon and inverse Radon transformation.

In contrast to the FBP there is no integral computation along the line detector (incl. limited sampling due to its element size) but an optional over-sampling along the numerous projection angles. One of DIRECTT's unique characteristics is its very *precise projection* of reconstruction elements taking into account their actual size and shape which is essential for enhanced spatial resolution. That is, reconstruction pixels are considered as a set of densely packed elements instead of being (circular smeared) point functions only. All previous calculations have been performed on base of square entries in a Cartesian matrix.

Position dependent smearing is implemented to the projection part of an iteration cycle exclusively. Fig. 4 (right) displays a screenshot of the crucial stages of the reconstruction algorithm DIRECTT: the model (A), the smear kernel as a function of position (B, the detector is placed on top), a 180° sinogram (C), which is filtered as described above (E) and reconstructed regardless of smearing (F). From the reconstruction obtained that way amplitudes of highest weights are selected (partial reconstruction G), which are exclusively added to the reconstruction sum (H). This intermediate reconstruction (H) is subject to projection again (taking into account the position dependent smearing) in order to get a computed sinogram, which subtracted from the original sinogram. The resulting residual sinogram (D) is the input for the subsequent iteration cycle (E' to H'), generates (D') and so forth.

4 Model reconstruction

As an example we chose a binary model (Fig. 3 left) whose motifs allow for assessment of certain reconstruction criteria such as the resolution of lines (substructured squares), homogeneity of flat surfaces and the sharpness of edges of the triangles and squares.

Fig. 5 (top) displays three 360° sinograms obtained from an unsmeared projection and projections using a constant and a position dependent smear kernel (from left to right, cf. Fig. 3). The Filtered Back-Projection (neglecting any type of smearing) yields the results depicted at the bottom: a sharp image superimposed by artifacts for the unsmeared sinogram, a blurred image for the constantly smeared projection and an even more blurred reconstruction for the variably smeared projection. (Employing the standard DIRECTT algorithm for the reconstruction of the unsmeared sinogram yields a result, which can hardly be differentiated from the original model.)

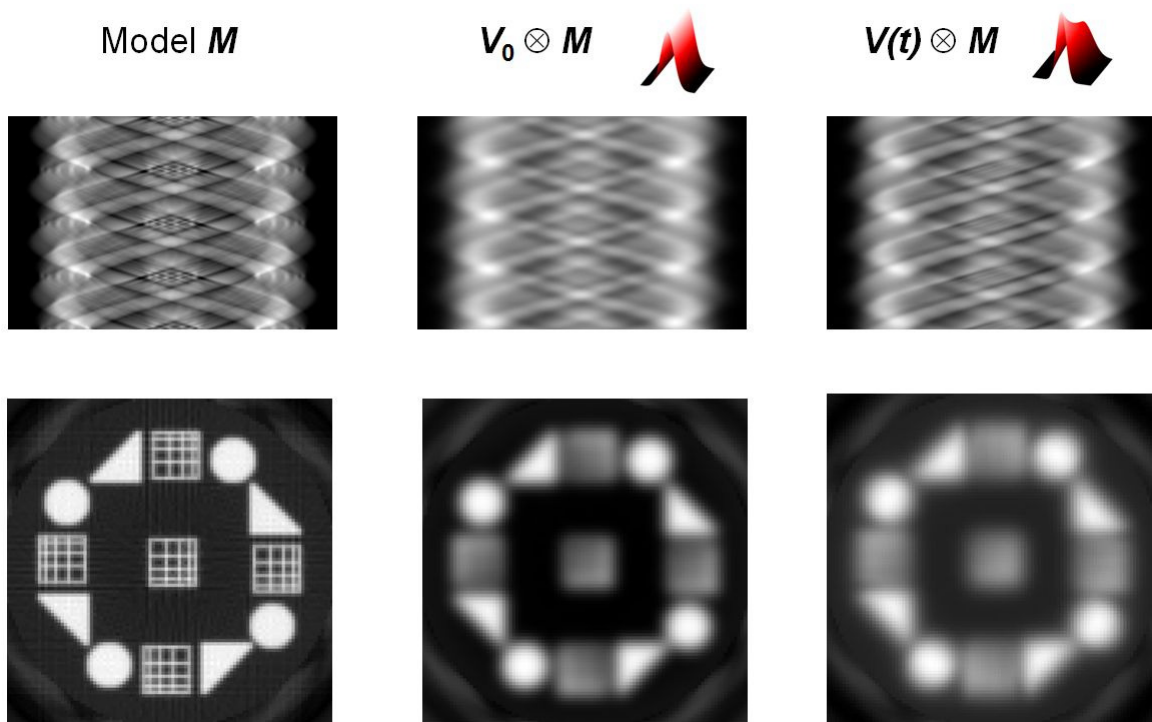


Fig. 5: Sinograms ($360 \times 1^\circ$) and the respective FBP reconstructions neglecting focal smearing (smear functions according to Fig. 3).

In light of these unsatisfactory results of FBP reconstructions the question arises, what gain of resolution can be yielded taking into account focal smearing. Is it sufficient to deconvolve the smeared projections from a constant kernel, or is there a further gain of resolution applying the proper position dependent smearing?

Figs. 6 and 7 emphasize the tremendous improvement of reconstruction quality when implementing smeared projecting into the DIRECTT algorithm (here we make use of the contrast criterion only).

The top line of Fig. 6 displays the model, the variable smear function and a 180° sinogram (position dependent smearing using Gaussian profiles of standard deviations $V=1$ to 5 , i.e. FWHM=2.5 to 12 pixels). Therefore the motifs of the model are subject to different degrees of smearing, depending on the range of positions they pass during the half rotation. Taking the right-hand square as example: it is in the 'sharp' half plane (i.e. above the horizontal line, where the actual smearing is less than the average) for all angles of projection considered. Even the (non-iterative) FBP shows that those motifs are reconstructed sharper.

On the bottom left we display the results of iterative reconstruction using different constant smear kernels (the extreme values $V=1$ and 5 and the mean $V=3$). Reconstructing with a small smear width emphasizes the flat surface motifs, while larger widths preferentially detect the highly contrasted edges. The best reconstruction result yields the proper position dependent variable smearing. However, for as few as 20 iterations (used here) spatial resolution on the left and right-hand side of the model still remains visible.

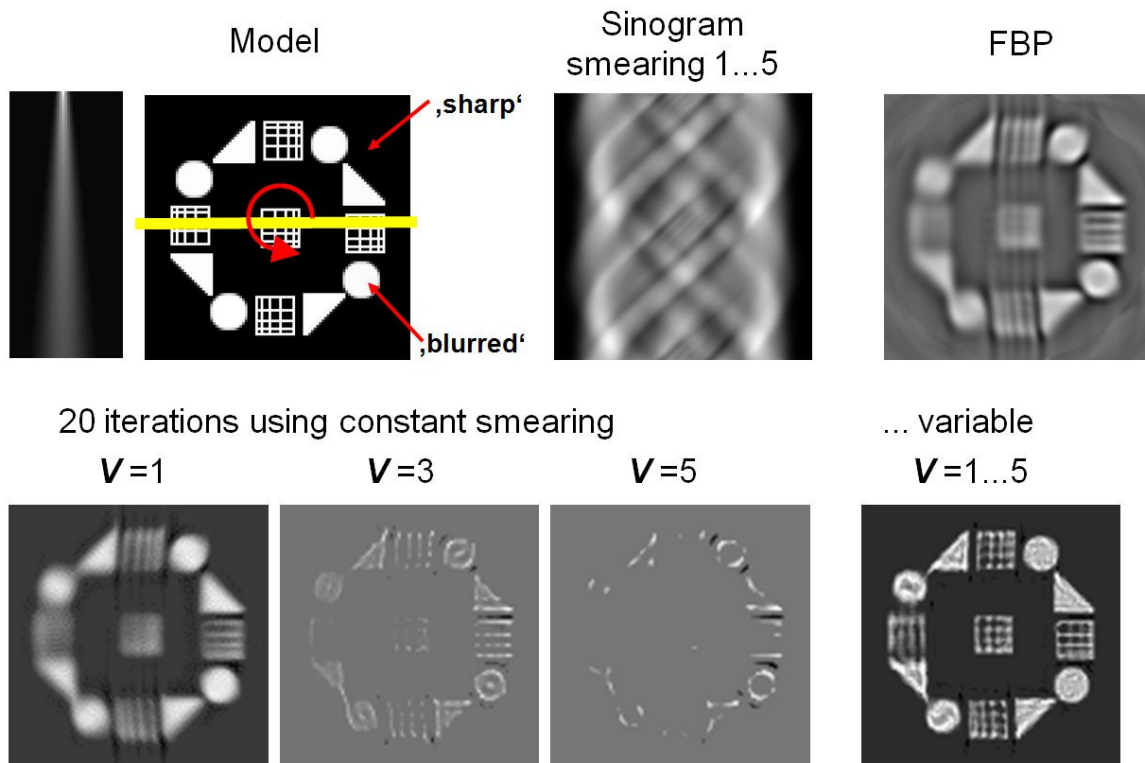


Fig. 6: Variable smear function, model and a 180° sinogram generated using focal smearing as a function of position and comparison of DIRECTT reconstruction results without iteration (top right), after 20 iterations using constant smear kernels V (bottom left) and variable focal smearing (bottom right).

In the 360° sinogram (Fig. 7) with the identical variation of (Gaussian) smearing none of the motifs is preferred. The FBP (no iteration) leads to a blurred reconstruction image again. Due to the doubled number of projections artifacts are reduced (as well as distortions) with respect to the results of the 180° reconstruction (Fig. 6). At the bottom line comparison is drawn for three representative reconstructions using projections of constant smear widths of standard deviations 1 to 5 pixels. The results are in complete correspondence to the 180° sinogram. Again, the best image quality regarding resolution is obtained from the reconstruction using the proper position dependent smearing.

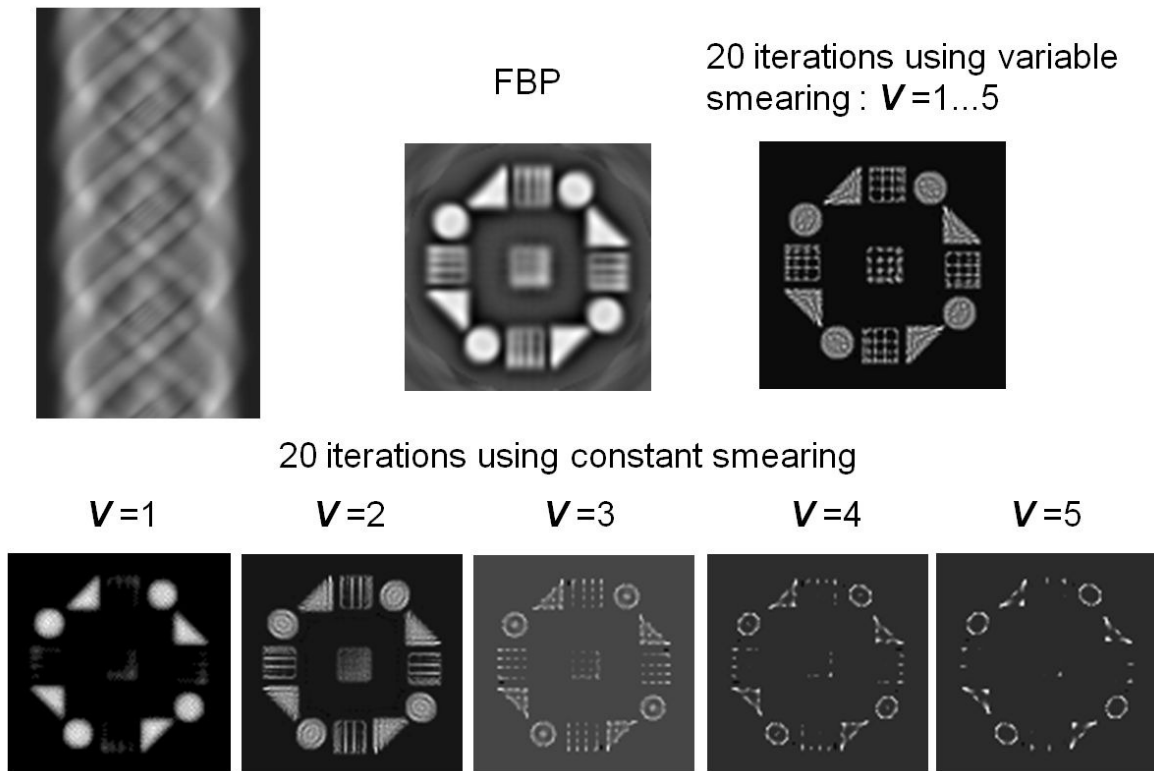


Fig. 7: 360° sinogram generated from position-sensitive smeared model projections and comparison of DIRECTT reconstruction results without iteration (top centre), after 20 iterations using constant smear kernels V (bottom) and variable focal smearing (top right).

Acknowledgements

Financial support by the German Federal Ministry for Education and Research (BMBF) in the network project “RuN-PEM” under contract no.: 03SF0324B is gratefully acknowledged. The authors like to thank the members of the working group „Bildgebende Verfahren“ at the Helmholtz-Zentrum Berlin für Materialien und Energie for splendid collaboration and open-minded discussion.

References

- [1] Handbook of Fuel Cells - Fundamentals, Technology and Applications, John Wiley & Sons, Chichester (2003).
- [2] C. Hartnig, R. Kuhn, P. Krüger, I. Manke, N. Kardjilov, J. Goebbels, B.R. Müller, H. Riesemeier: Wassermanagement in Brennstoffzellen - die Bedeutung von hochauflösenden zerstörungsfreien Untersuchungsmethoden. *MP Materials Testing* **50** (10) (2008) 609-614.
- [3] I. Manke, C. Hartnig, N. Kardjilov, A. Hilger, A. Lange, A. Kupsch, J. Banhart: Wasserverteilung in PEM-Brennstoffzellen. *MP Materials Testing* **51** (4) (2009) 219-226.
- [4] Patent DE 103 07 331 (05.03.2009).
- [5] A. Lange, M.P. Hentschel, A. Kupsch: Computertomographische Rekonstruktion mit DIRECTT: 2D-Modellrechnungen im Vergleich zur gefilterten Rückprojektion. *MP Materials Testing* **50** (5) (2008) 272-277.

- [6] A. Lange, M.P. Hentschel, A. Kupsch: True 3D-CT-reconstruction in comparison to the FDK-algorithm, Proceedings 17th World Conference on Non-Destructive Testing (2008).
- [7] A.C. Kak; M. Slaney: Principles of computerized tomographic imaging, Classics in Applied Mathematics **33**, siam (2001) and IEEE Press, New York (1988).
- [8] J. Radon: Über die Bestimmung von Funktionen längs gewisser Mannigfaltigkeiten. Berichte der math.-phys.Kl. Sächsischen Gesellschaft der Wissenschaften **59**, Leipzig (1917) 262.